AOARD PROJECT REPORT

ENTITLED

Super Resolution Imaging Applied to Scientific Images

Principal Investigator

Prof. S. Chaudhuri

Dept. of Electrical Engineering,

I.I.T., Bombay

Report Documentation Page

Form Approved
OMB No. 0704-0188

1. REPORT DATE	2. REPORT TYPE	3. DATES COVERED
06 JUL 2007	**FInal**	**25-04-2006 to 26-06-2007**

4. TITLE AND SUBTITLE	5a. CONTRACT NUMBER
Joint Research on Super Resolution imaging applied to Scientific Images	**FA48690610043**
	5b. GRANT NUMBER
	5c. PROGRAM ELEMENT NUMBER
6. AUTHOR(S)	5d. PROJECT NUMBER
Subhasis Chaudhuri	5e. TASK NUMBER
	5f. WORK UNIT NUMBER
7. PERFORMING ORGANIZATION NAME(S) AND ADDRESS(ES)	8. PERFORMING ORGANIZATION REPORT NUMBER
Indian Institute of Technology, Bombay,Dept. of Electrical Engg., IIT Powai,Mumbai 400 076 India,IN,400 076	**N/A**
9. SPONSORING/MONITORING AGENCY NAME(S) AND ADDRESS(ES)	10. SPONSOR/MONITOR'S ACRONYM(S)
AOARD, UNIT 45002, APO, AP, 96337-5002	**AOARD**
	11. SPONSOR/MONITOR'S REPORT NUMBER(S)
	AOARD-064025

12. DISTRIBUTION/AVAILABILITY STATEMENT

Approved for public release; distribution unlimited

13. SUPPLEMENTARY NOTES

14. ABSTRACT

Super-resolution refers to the process of producing a high spatial resolution image than what is afforded by the physical sensor through post processing means. It includes up sampling the image, thereby increasing the maximum spatial frequency, and removing degradations that arise during the image capture, viz., aliasing and blurring. Various methods have been explored for super resolution of material surface images as well as other images in the report. Based on observations it is recommended to use either the contourlet based method or TV based approach for super-resolving optical microscope data. To super-resolve the AFM data, it is recommended to use either TV-based approach or PG method.

15. SUBJECT TERMS

super resolution imaging, computer vision, Image Processing, Signal Processing, Data Fusion

16. SECURITY CLASSIFICATION OF:			17. LIMITATION OF ABSTRACT	18. NUMBER OF PAGES	19a. NAME OF RESPONSIBLE PERSON
a. REPORT	b. ABSTRACT	c. THIS PAGE			
unclassified	**unclassified**	**unclassified**	**Same as Report (SAR)**	**39**	

PREFACE

This document is the final report of the research conducted in accordance to the contract AOARD-06-4025. The project has been completed on May 1, 2007 as per the official contract. The draft of the final report is also completed by May 2007. The document contains the narration of the original problem, a technical description of the state-of-the-art as well as specific technical work conducted for this purpose. During the course of the research, intermediate versions of the code were dispatched to Prof. Guna Seetharaman, AFIT/ENG, who facilitated the testing on AFRL provided datasets and provided feedback. The final version of the code is being delivered along with this report. Also, the latest code and the results of the feasibility studies are being sent to the AFRL/ML collaborators. Dr. Seetharaman also visited IIT Bombay during April 16-30, 2007 on a related research mission and had an opportunity to verify and be trained on using the developed computer programs.

The contract was to investigate the feasibility of super resolution imaging of large surfaces at nano-scale resolution. Four different techniques were considered for this study, and the computational results indicate a promising performance with a peak PSNR gain of 6 db over standard bilinear interpolation. In some cases, even a scale factor of 4 produced reliable results. Specifically the effort included: (1) a thorough survey of the state of the art, (2) data collected by US collaborators and analyzed by the investigator, (3) development of Papoulis-Gerchberg method to implement the analytic continuation of spectral details, (4) exploration of contourlet and its variant known as the Laplacian Edge model. Additionally, we developed a new technique for super resolution of material images known as total variation optimized image interpolation. The deliverance of this report serves to meet the fifth objective of the original contract.

Place: Mumbai
Date: May 1, 2007

(Subhasis Chaudhuri)
Principal Investigator

Encl: Full report

1. Introduction:

In most imaging applications, images with high spatial resolution are desired and often required. However acquisition of high-resolution images is severely constrained by the physical drawbacks of the diffraction limited imaging sensors. The images acquired through such sensors suffer from aliasing and blurring. The most direct solution to increase the spatial resolution is to increase the number of pixels per unit area, by sensor manufacturing techniques. But due to decrease in pixel size, light available also decreases causing more shot noise. Another approach to increase the resolution is to increase the wafer size, which leads to an increase in the capacitance. This approach is not effective since an increase in the capacitance causes a decrease in charge transfer rate. Hence, a promising approach is to use image processing methods to construct a high-resolution image from one or more available low-resolution observations.

Super-resolution refers to the process of producing a high spatial resolution image than what is afforded by the physical sensor through post processing means. It includes up sampling the image, thereby increasing the maximum spatial frequency, and removing degradations that arise during the image capture, viz., aliasing and blurring.

2. Literature Review:

Numerous reconstruction-based super-resolution algorithms have been proposed in the literature. The idea of super-resolution was first proposed by Tsai and Huang, which used the frequency domain approach [1]. A different approach to the super-resolution restoration problem was suggested by Irani *et al* [2], [3] based on the iterative back projection method. A set theoretic approach to the super-resolution restoration problem was suggested in [4]. The main result there is to define convex sets which represent tight constraints on the solution to improve the results. Ng *et al* developed a regularized, constrained total least squares solution to obtain a high-resolution image [5]. They consider the presence of perturbation errors of displacements around the ideal sub-pixel locations in addition to noisy observations. The effect of the displacement errors on the convergence rate of an iterative approach for solving the transform based preconditioned system of equations is discussed by Ng and Bose [6]. They also develop a fast restoration algorithm for color images in [7]. Nguyen proposed circulant block preconditioners to accelerate the conjugate gradient descent method while solving the Tikhonov-regularized super-resolution problem [8]. A maximum *a posteriori* (MAP) estimator with Huber-Markov

random field (MRF) prior is described by Schultz and Stevenson in [9]. Other approaches include a MAP-MRF based super-resolution technique using the blur as a cue [10]. In [11] the authors recovered both the high-resolution scene intensity and the depth fields simultaneously using the defocus cue. Elad and Feuer [12] proposed a unified methodology for super-resolution restoration from several geometrically warped, blurred, noisy and down-sampled measured images by combining maximum likelihood (ML), MAP and projection onto convex sets (POCS) approaches. In [13] Lin and Shum determine the quantitative limits of reconstruction-based super-resolution algorithms and obtain the up-sampling limits from the conditioning analysis of the coefficient matrix.

Now we review some of the recent works under the learning-based super-resolution category. In [14] Baker and Kanade develop a super-resolution algorithm by modifying the prior term in the cost to include the results of a set of recognition decisions, and call it recognition-based super-resolution or hallucination. Their prior enforces the condition that the gradient in the super-resolved image should be equal to the gradient in the best matching training image. Authors in [15] have proposed a super-resolution technique from multiple views using learned image models making use of principal component analysis (PCA). Their method uses learned image models either to directly constrain the maximum likelihood (ML) estimate or as a prior for a MAP estimate. In [16] Freeman proposed a parametric Markov network to learn the statistics between the “scene" and the “image", as a framework for handling low level vision tasks, one application of which is super-resolution. An image analogy method applied to super-resolution is discussed in [17].

Joshi and Chaudhuri [18] have proposed a learning-based method for image super-resolution from zoomed observations. They model the high-resolution image as a Markov random field (MRF), the parameters of which are learned from the most zoomed observation. The learned parameters are then used to obtain a maximum *a posteriori* (MAP) estimate of the high-resolution image.

In [19] we have proposed a single frame super-resolution algorithm using a wavelet-based learning technique where the HR edge primitives are learned from the HR data set locally. An eigen face-domain super-resolution reconstruction algorithm for face recognition is proposed in [20]. In the face hallucination technique proposed in [21] the authors use both low and high resolution image databases to recover the high-resolution image, making use of PCA. They also add constraints to the principal components to reduce the nonface-like distortion. The use of PCA for image zooming purposes has been investigated in [22]. It has been assumed that the principal components remain unchanged across the scale. The method is applicable only to

zooming up of images of a specific class of objects such as faces or fingerprints. Pickup *et al.* [23] present a domain-specific image prior in the form of a distribution function based upon sampled images, and show that for certain types of super-resolution problems, this sample-based prior gives a significant improvement over other common multiple-image super-resolution techniques.

In [24] the authors have proposed a single frame image super-resolution method where the generation of the high-resolution image patch depends simultaneously on multiple nearest neighbors in the training set in a way similar to the concept of locally linear embedding for manifold learning. This method requires fewer training examples than other learning-based super-resolution methods. The super-resolution method proposed in [25] is the extension of a Markov-based learning algorithm, capable of processing an LR image with unknown degradation parameters. A different method for enhancing the resolution of LR facial images using an error back projection method based on top-down learning is proposed in [26]. Here a face is represented by a linear combination of prototypes of shape and texture. An image hallucination approach based on primal sketch priors is presented in [27]. Here a reconstruction constraint is also applied to further improve the quality of the hallucinated image.

In [28] the super-resolution reconstruction problem is considered as a binary classification problem and is solved through class conditional probability estimation. Most of the learning-based super-resolution methods proposed above either make use of a database of low and high resolution training images of similar objects or use an appropriate smoothness constraint along with the learning prior to improve the results. In our method we use instead an arbitrary set of high-resolution training images. Also we do not use any smoothness constraint as we apply the contourlet transform which has the capability to capture smoothness along contours, while learning the best edge primitives from the HR training set. The proposed method is edge-based and involves learning the edge pattern locally instead of the global PCA based approach. As a result, our method is faster and results show considerable improvement over a regularization-based approach. In [29] we have proposed total variation based regularization framework for Image super-resolution. Total variation based regularization helps in formulating an edge preserving scheme. This formulation is extended by incorporating an appropriate sub-band constraint ensures the preservation of textural details in trade off with noise present in the observation.

In [30] we make use of Papoulis-Gerchberg algorithm of signal extrapolation to perform Image super-resolution the same algorithm is later modified to handle blurred image. In [31] author uses a generative model for sharp edges in images as

well as descriptive models for edge representation. This prior information is injected using the symmetric residue pyramid scheme. The advantages of this scheme are that it generates sharp edges with no ringing artifacts in the HR and that the models are universal enough to allow usage on wide variety of images without requirement of training and/or adaptation.

3. Methods Explored:

We have mainly investigated learning based algorithms for obtaining the super-resolution on scientific images. Methods implemented explore both the frequency domain and spatial domain. We started with learning priors for performing super resolution and towards the end; we also implemented super resolution in frequency domain. For contourlet based approaches, we have used a training database consisting of high resolution images. For Papoulis-Gerchberg method number of iterations and the filter used both govern the achievable performance of super-resolved image at the output.

The Super-resolution method gives good results. Here only a single low resolution image is used. For Edge model based high resolution image generation technique also, a single low resolution image is required thus, no training or high resolution exemplars are required.

We have explored the following methods of super resolution in this report.

- Wavelet based approach
- Contourlet based approach
- Papoulis Gerchberg algorithm
- Edge Model based method
- Total Variation approach

3.1. Wavelet Based Approach:

We attempt to solve the super-resolution problem using a learning based method. Since the problem of super-resolution involves handling data at multiple resolutions, and since the wavelets are best suited for a multi-resolution analysis, it motivates us to use a wavelet based approach for learning the wavelet coefficients at the finer resolution. By using a wavelet-based learning prior along with a suitable discontinuity preserving smoothness prior, an effective super-resolution can be achieved. The advantage of this method is that there is no correspondence problem. Further, one does not need multiple observations, but it does require a number of high resolution training images.

The method proposed here can also be classified under learning based super-resolution schemes. However, we use a different type of learning where we use a prior term that enforces the condition that the wavelet coefficients of the super-resolved image at the finest scale should be locally close to the best matching wavelets learnt from the high resolution training set. We obtain a regularized solution by imposing an appropriate smoothness constraint (on the restored image) which ensures the spatial correlation among the pixels while preserving the discontinuities.

The basic problem we solve is as follows: one captures an image using a low-resolution camera. We are interested in generating the super-resolved image for the same using a set of available high-resolution images of different scenes. It is assumed that the high frequency contents to be extrapolated are locally present in the training set. We use a wavelet based multi-resolution analysis to learn the wavelet coefficients at a given location at the finer scales for the super-resolved image. The learnt coefficients are then used in a prior term that enforces the condition that the wavelet coefficients at the finer scales of the super-resolved image should be locally close to the best matching coefficients learnt from the training set. In order to preserve the spatial continuity of the restored image, we use a smoothness constraint in conjunction with the learnt prior to obtain the super-resolved image.

3.1.1. Wavelet Based Learning:

Wavelets are mathematical functions that split up data into different frequency components locally, and then study each component with a resolution matched to its scale. They have advantages over traditional Fourier transform based methods in analyzing physical situations where the signal contains discontinuities or a local analysis is required. In the case of DWT, filters of different cut off frequencies are employed to analyze the sequence at different scales.

The input sequence is passed through a series of high-pass and low-pass filters to analyze the high and low frequency components, respectively. The filtered output is then sub-sampled by a factor of 2 simply by discarding every other sample. The low-pass filter thus halves the resolution, but leaves the scale unchanged. The subsequent sub-sampling by a factor of 2, however, changes the scale.

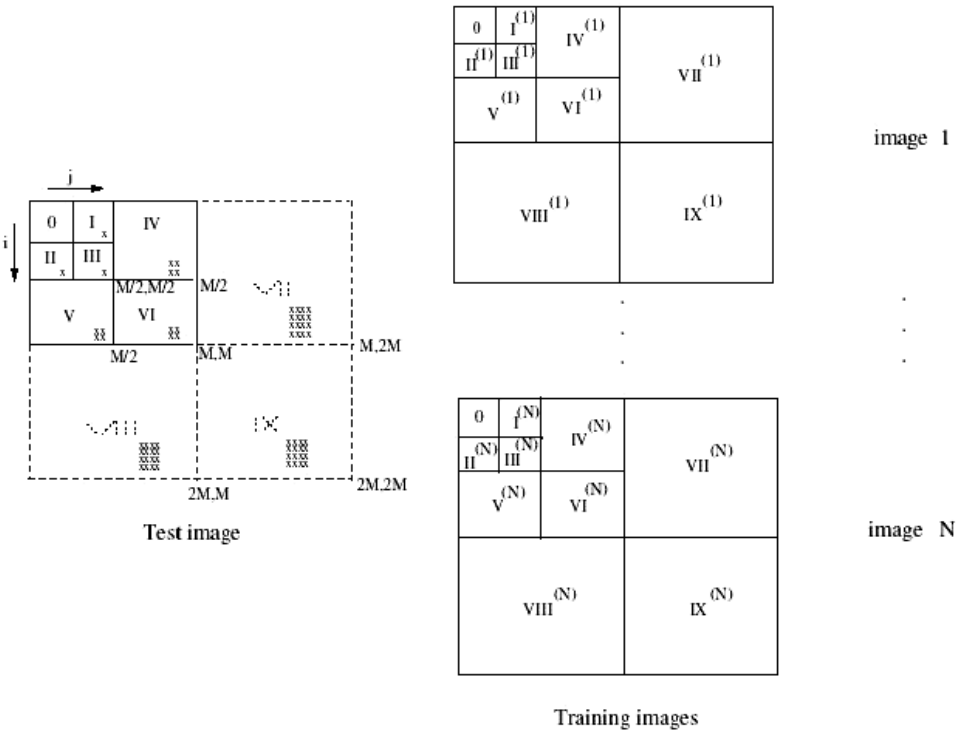

(a) (b)

Fig. 1 Illustration of learning of wavelet coefficients at a finer scale: (a) Low resolution image with two level decomposition. Wavelet coefficients (marked as x) in sub-bands shown with the dotted lines are to be estimated for bands VII –IX. (b) high resolution training set in wavelet domain with 3-level decomposition.

For our problem the low resolution image is of size *MxM* pixels (Refer Fig.1). Considering an up-sampling factor of 2, the high-resolution image, now has a size of *2Mx2M* pixels. For each coefficient in the sub-bands *I- III* and the corresponding *2x2* blocks in the sub-bands *IV-VI*, we extrapolate a block of *4x4* wavelet coefficients in each of the sub-bands *VII, VIII and IX as* shown in Fig.1. We follow the minimum absolute difference (MAD) criterion to estimate the wavelet coefficients. We take the absolute difference locally between the wavelet coefficients in the low resolution image and the corresponding coefficients in each of the high resolution training images.

3.1.2. Sample Results:

We now show results of an experiment conducted on the color face images. We observe that the super-resolved image appears sharper, as shown in fig.2 below.

(a) (b) (c)

Fig. 2(a) A low resolution face image of size MxN, (b) 2Mx2N sized bicubic interpolated Image of (a), (c) 2Mx2N sized super-resolved image of (a) by wavelet based technique.

As shown in fig.2 (a) above a low resolution image is of size MxN is better reconstructed by wavelet based technique. Observe the eye balls, eye brows, frontal hair, and the nose shown in fig.2 (c) which appear sharper when compared to the bicubic interpolated image given in fig.2 (b).

Fig. 3 shows results of an experiment conducted on an image of a building, having well defined vertical and horizontal edges. The super resolved image is definitely sharper than the bicubic-interpolated image as shown below. However, one does notice certain blockiness in the reconstructed images.

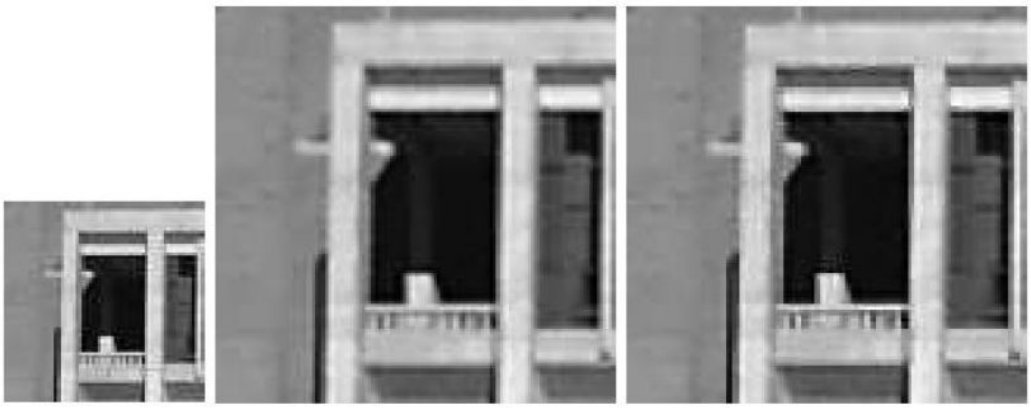

(a) (b) (c)

Fig.3.Result of wavelet based method on a sample image of a building by factor 2: (a) low resolution image, (b) bicubic interpolated image, (c) super-resolved image.

3.1.3. Regularization of wavelet based method:

Since we pick up the high frequency components of each *8x8* region as per the best-fit edge element from different training data independently, there is no guarantee that the corresponding high-resolution image would be a good one as it lacks any spatial context dependency, leading to blockiness in the resulting image. We must use a smoothness constraint.

Now, in order to enforce the smoothness constraint we make use of the fact that the image pixel intensities have a spatial correlation. This prior knowledge serves as a contextual constraint and has to be used to regularize the solution. But this constraint pushes the reconstruction towards a smooth entity. Hence in order to enforce smoothness in the smooth regions alone while up sampling, we use a discontinuity preserving smoothness prior. Since the high frequency details learnt by using the wavelet based prior constitute the discontinuities it would ensure undistorted edges in the super-resolved image while smoothing the regions with spatial continuity.

The prior for the smoothness constraint in this study is:

$$U(\mathbf{z}) = \sum_{(ij)} \{\mu[(z_{(ij)} - z_{(ij-1)})^2 (1-v_{(ij)}) + (z_{(ij+1)} - z_{(ij)})^2 (1-v_{(ij+1)}) + (z_{(ij)} - z_{(i-1,j)})^2 (1-l_{(ij)}) + (z_{\{i+1,j\}} - z_{\{i,j\}})^2 (1-l_{\{i+1,j\}})] + \gamma(l_{\{i,j\}} + l_{\{i+1,,j\}} + v_{\{i,j\}} + v_{\{i,j+1\}}) \quad \ldots (1)$$

We denote the high resolution (HR) image by z.

Here μ is the penalty term for departure from the smoothness, and l and v are the binary line fields denoting horizontal and vertical discontinuities. Let $Z_{\omega t}$ be wavelet transform of the high resolution image to be estimated and $\hat{Z}_{wt}$ be the wavelet transform of the learnt image. Then the wavelet prior can be expressed as

$$C(z) = \left\| Z_{wt} - \hat{Z}_{wt} \right\|^2 \quad \ldots (2)$$

Thus by making use of the data fitting term, the learning term and the smoothness constraint, the final cost function to be minimized for the high resolution image **z** can be expressed as

$$\varepsilon = \| \mathbf{y} - D\mathbf{z} \|^2 + \beta C(z) + U(z) \quad \ldots (3)$$

where D is the decimation matrix and **y** is the observed image.

The first term relates to the consistency in data fitting. The second term gives the learning term and the third term gives the smoothness constraint. We minimize the cost by using the simulated annealing technique, which possibly leads to a global minimum. We illustrate the result obtained using the regularization process in fig.4.For better visual interpretation, we cropped eye of super-resolved tiger face. One does observe a sizeable improvement due to regularization. Eye of super resolved tiger image as shown in fig.4 (g) looks sharper than fig.4 (e).

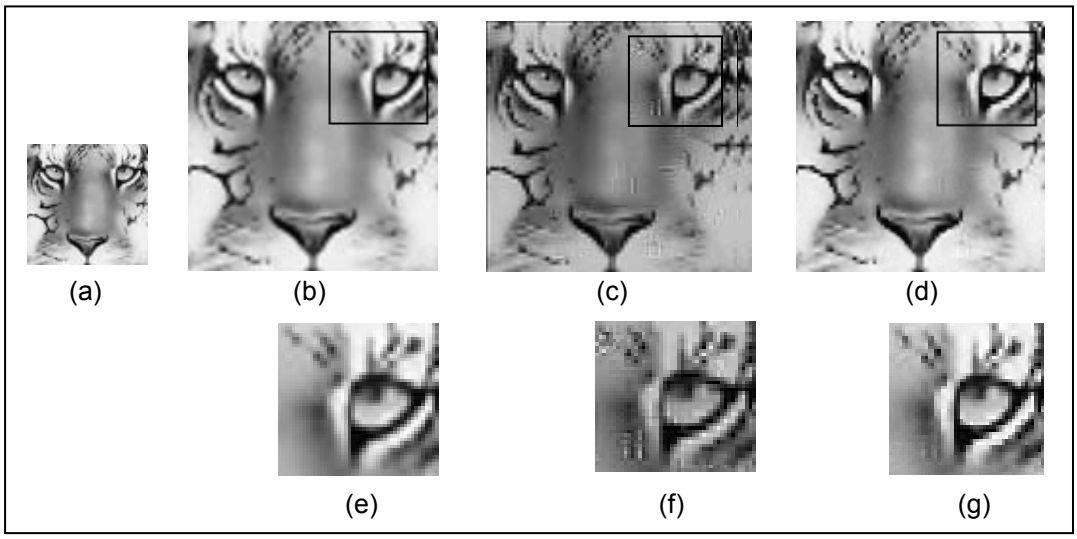

Fig. 4 (a) low resolution image, (b) bicubic interpolated image and its cropped part is shown in (e), super-resolved by wavelet approach (without regularization) shown in (c) and its cropped part is shown in (f), super-resolved by wavelet (with regularization) shown in (d) and its cropped part is shown in (g).

However, the computation becomes extremely slow. In the next section we show that similar quality of results, of not any better can be obtained using contourlet transform. Instead of wavelet transform which does not require any regularization. Hence we do not pursue this method any longer for superresolving images of material surfaces

3.2. Contourlet based approach

One of the major difficulties with wavelet-based learning lies in the fact that most implementation employs wavelet decomposition using separable kernel along x and y directions. Although this provides computational advantages, we expect to catch only the horizontal and vertical edges properly. Hence we do not have difficulties in learning horizontal and vertical edges, but we do have some problem in learning edges oriented along arbitrary directions. This give rise to certain artifacts in the reconstructed image and in order to get a good quality super-resolved image we were forced to use an appropriate discontinuity preserving smoothness constraint under a regularization framework. Thus we ensure spatial correlation among pixels using the smoothness constraint, as well as obtain the best matching edges from the training set using wavelet learning. This requires a stochastic optimization technique to obtain the solution which made the reconstruction process very slow.

A better way to handle the above situation is to use directionally selective wavelet decomposition to learn the oriented edges where the reconstruction problem need not be solved under a regularization framework, resulting in a much faster solution.

This motivated us to use the contourlet transform [32], which is capable of catching the smoothness along contours, naturally.

3.2.1. Contourlet Transform:

The contourlet transform retains the multi-scale and time-frequency localization properties of wavelets. In addition, it also offers a high degree of directionality. Thus they are capable of capturing the geometrical smoothness of the contour along any possible direction. The contourlet transform is implemented in two stages: the sub-band (spectral) decomposition stage and the directional decomposition stage. For the sub-band decomposition stage we use the Laplacian pyramid where the decomposition at each step generates a sampled low-pass version of the original and the difference between the original image and the prediction. The directional filter bank (DFB) is efficiently implemented by using an *m*-level binary tree decomposition that leads to 2^m sub-bands with wedge-shaped frequency partitioning. Combining the Laplacian pyramid and the directional filter bank yields the discrete contourlet transform.

3.2.2. Learning of Edge Primitives:

We plan to learn the mapping of an LR edge (called edge primitive here) to its HR representation locally from the training data set during up sampling. Since wavelets are known to capture the high frequency details very well locally, we propose to use contourlets to learn this mapping. We use a contourlet based learning technique where the HR edge primitives are learned from the HR data set locally with the assumption that a primitive edge element in the HR image is localized to an *8x8* pixel area, and the corresponding edge elements over a *4x4* pixel area in the LR image. Each local region is learned independently from the HR data set.

3.2.3. Learning the Contourlet Coefficients:

Given a low-resolution input image *y*, we perform a contourlet decomposition consisting of two pyramidal levels and each pyramidal level is then decomposed into four directional sub-bands which yield the decomposition. A three level decomposition is performed on all the high resolution database images and each pyramidal level is decomposed into four directional sub-bands. Our idea is to learn the contourlet coefficients in the four directional sub-bands corresponding to the finest level for the given low resolution image. After learning, we have a three level decomposition for the input image, i.e., the original low level decomposition coefficients plus the learned coefficients at the finer scale. The inverse transform of this will yield the high resolution equivalent of the low resolution input.

Here the low-resolution image is of size *MxM* pixels. Considering an up sampling factor of 2, the high-resolution image, now has a size of *2Mx2M* pixels. For each coefficient in the sub-bands *I - IV* and the corresponding *2Mx2M* blocks in the sub-bands *V- VIII* we extrapolate a block of *4x4* contourlet coefficients in each of the sub-bands *IX, X, XI* and *XII* [refer Fig. 5].

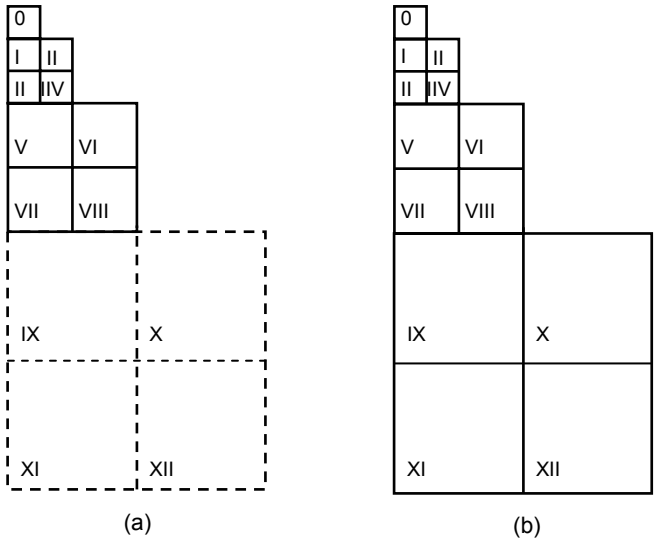

Fig. 5 Illustration of learning contourlet coefficients at a finer scale: (a) A low-resolution image with two-level decomposition. Coefficients in dotted sub-bands are to be learnt. (b) A representative high-resolution training set in contourlet domain with three-level decomposition.

In order to do this we exploit the idea from zero tree concepts, i.e., in a multiresolution system, every coefficient at a given scale can be related to a set of coefficients at the next coarser scale of similar orientation. Using this idea we follow the minimum absolute difference (MAD) criterion to estimate the contourlet coefficients. We take the absolute difference locally between the contourlet coefficients in the low resolution image and the corresponding coefficients in each of the high resolution training images. This is repeated for each coefficient in sub-bands *I, II, III* and *IV* of the low resolution image. In effect, we find the best matching *8x8* edge primitive from the training data for a given *4x4* representation in the low-resolution image through contourlet expansion.

In our experiments we used ``9-7" biorthogonal filters for the Laplacian pyramid because they are close to being orthogonal and also because of their linear phase characteristics. For the directional filter banks we used the “23-45" biorthogonal quincunx filters and modulate them to obtain the biorthogonal fan filters. These filters are also nearly orthogonal and have linear phase response. The complete learning-based resolution enhancement procedure is summarized below in terms of the steps involved.

3.2.4. Sample Results:

Fig.6(c) shows the result of the corresponding experiments conducted on an LR textured image shown in Fig.6 (a). The super-resolved image using the proposed approach is observed to be much sharper compared to the results of bicubic interpolation. In particular, the edges are better preserved in the super-resolved image using contourlet learning than the bicubic interpolated image where it appears to be more blurred. The super-resolved image compared very favorably to the original high-resolution image shown in Fig.6 (b). For all these experiments the database of HR images comprised of a collection of 64 arbitrary images of both indoor and outdoor scenes.

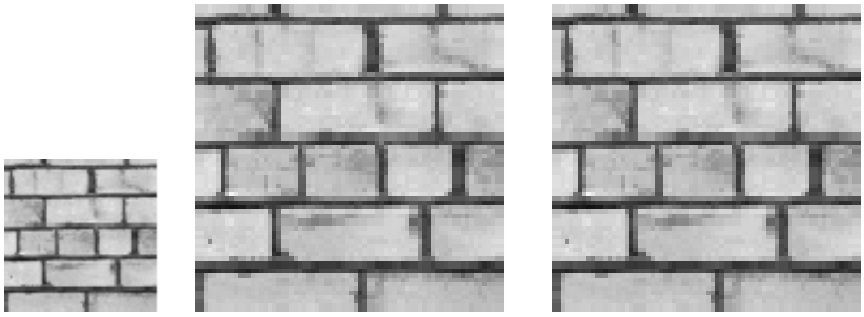

(a) (b) (c)

Fig. 6 (a) A low resolution texture image, (b) corresponding HR image, (c) the super-resolved image using the contourlet learning.

Now we show the results of the experiments performed on a LR image where the aliasing is very high. The purpose of this experiment is to demonstrate the behavior of the proposed method when severe aliasing is present in the LR data. Such a low resolution image is shown in Fig. 7(a) and the corresponding bicubic interpolated image is shown in Fig. 7(b).

(a) (b) (c)

Fig. 7 (a) a low resolution image with prominent aliasing, (b) bicubic interpolation of low resolution image, (c) The super-resolved image using contourlet learning.

Note that the stripes on the scarf are aliased. The super-resolved image using the proposed approach is shown in Fig. 7(c). The super-resolved image appears to be

much sharper than the bicubic interpolated one. However, the proposed method was unable to remove the aliasing effect.

3.3. Super resolution using Papoulis-Gerchberg method

3.3.1. Papoulis-Gerchberg method

This method of super-resolution is based on the work done independently by Papoulis [33] and Gerchberg [34]. The motivation for their work was signal extrapolation from only a part of the original signal i.e. determination of the transform

$$F(w) = \int_{-\infty}^{+\infty} f(t)\, e^{-jwt}\, dt \qquad \ldots (4)$$

of a signal f(t) given a finite segment

$$g(t) = f(t)PT(t), \qquad where\ \ PT(t) = \begin{cases} 1, & |t| \le T \\ 0, & |t| > T \end{cases} \qquad \ldots (5)$$

The signal extrapolation is carried out by the method of alternate projections [35], iterating alternately between time and spectral domains. The signal *g(t)* is low-pass filtered by truncating its Fourier transform outside the interval [-σ; σ], assuming σ is the signal bandwidth of *f(t)*. In the n^{th} iteration this can be expressed as

$$F_n(w) = G_{n-1}(w)P_\sigma(w),\ P_\sigma(w) = \begin{cases} 1, & |w| \le \sigma \\ 0, & |w| > \sigma \end{cases} \qquad \ldots (6)$$

The inverse function of $F_n(\omega)$ is then computed as $f_n(t)$. This results in a reduction of the error signal $|f(t) - f_n(t)|^2$ outside the known segment of the signal. This follows from Parseval's theorem. However, the signal $f_n(t)$ does not match the observed signal *g(t)* in the region [-T, T]. This part of the signal is then restored to the original known segment forming the function $g_n(t)$ for the next iteration.

$$g_n(t) = f_n(t) + \left[f(t) - f_n(t) \right] PT(t) = \begin{cases} g(t), & |t| \le T \\ f_n(t), & |t| > T \end{cases} \qquad \ldots (7)$$

This process is then iterated with the new $g_n(t)$. In each iteration the mean square error of the extrapolated signal is reduced two folds. Hence with successive iterations the generated extrapolated signal approaches the desired signal *f(t)*. Convergence of the method is guaranteed and is shown in [33]. However, the process ideally requires an infinite number of iterations. If we stop after r iterations, the reconstructed signal is given by $f_r(t)$ instead of f(t). Also, in practical cases the measured data g (t) = $g_0(t)$ will contain error. The propagation of this measurement error can be controlled by early termination of the iterative process [34, 36]. The process also assumes the signal f(t)

to be band limited, but it is found that the method works reasonably well for signals with sufficiently low energy in their higher frequency components.

3.3.2. Application to Super-resolution (SR)

The low-resolution image is projected on a higher dimensional grid (taking the factor of zoom into consideration) where the values of some pixels are known and some are unknown. The unknown pixel values are initially set to zero. In the next step, the image is taken to its frequency domain and the higher frequencies are taken to zero. This is low-pass filtering the image. After this step, the unknown pixels will have some values. But, the known pixel values have changed as a result of the filtering. In the next step, these values are set back to their original values, creating the higher frequency components. The whole process is repeated. Fig.8 compares output of the method after 50 iterations with that of the bicubic interpolation.

(a) (b) (c)

Fig. 8 (a) Low resolution Lena image, (b) bicubic interpolated image, (c) super-resolved image by PG method.

Though the method is quite fast it has some drawbacks. It relies heavily on the fact that the measured (known) pixel values are the values that are to be obtained in the reconstructed high-resolution image. In other words, it assumes that the low-resolution images are down-sampled versions of the expected high-resolution image. Hence, it is not able to compensate effectively for blur and noisy measurement of data. We overcome this drawback by introducing a different constraint enforcing part. We want to enforce that the super-resolved image obtained after every iteration of method confirms to the input low resolution image. To do this we introduced a back projection part within the PG method. Iterative back projection has been used in image super-resolution by Irani and Peleg [2]. Here we deal with case when only single LR image is available. In our model after every iteration of the PG model we calculate the error between the LR image and simulated LR image formed by

applying the known decimation model to the obtained SR image, mathematically, the error e_i can be expressed as

$$e_i = y - Dz_i \quad \ldots (8)$$

Where *y* is the input LR image, *D* is the decimation matrix that we assume to be known to us and z_i is the obtained SR image after the i^{th} iteration of the method. We then compensate for the error in the obtained SR image by adding the error for each pixel of the simulated LR image to the corresponding block of pixels in the obtained SR image. We then proceed with next iteration. It may be noted here that due to this error compensation in blocks certain blockiness will be introduced to the SR image obtained at this point. However, this is then taken care of in the low-pass filtering part of next iteration. The algorithm terminates when the error is small enough. This method may thus seem as a process where we attempt to reverse the process of averaging as shown in fig.9 below.

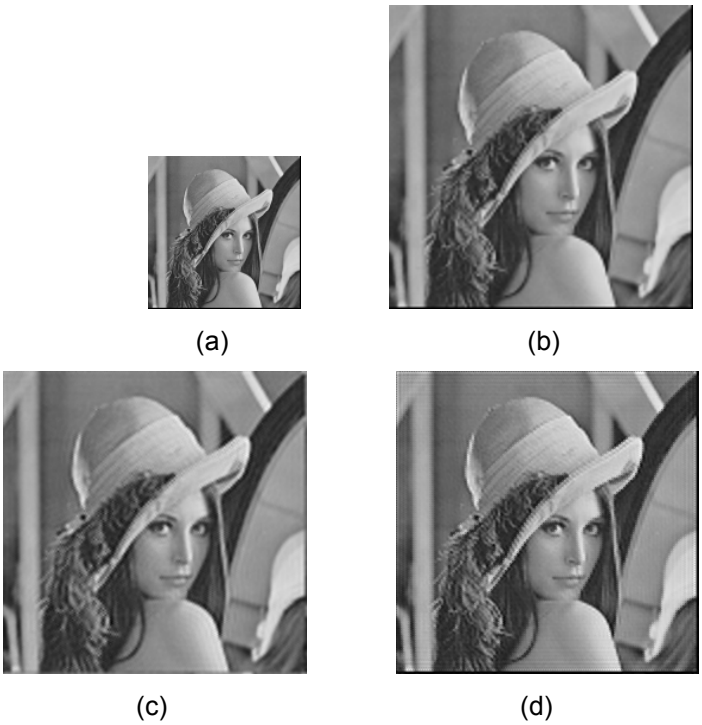

(a) (b)

(c) (d)

Fig. 9 super-resolution of Lena Image using PG method with deblurring: (a)Low resolution Lena image formed by averaging and downsampling of a high resolution image, (b)2x zoomed image using bicubic interpolation, (c)super-resolved image formed using the standard PG method, (d) super-resolved image formed using PG method with deblurring.

3.4 Edge Model Based Super-resolution

It has been shown in Edge-model based representation of Laplacian subbands that one can very efficiently model LR edges and synthesize their corresponding HR representation using a Laplacian Pyramid [37] instead of using contourlet as

explained in section 3.2. We refrain from reproducing them here for the purpose of brevity. The corresponding algorithm has been implemented and the results of application on images of material surfaces are given in next section.

3.5 Total variation based approach

The image formation model for the low resolution image from a high resolution image is given as

$$y(x) = d(x)(h * z) + n(x) \quad \ldots (9)$$

Here, $d(x)$ is the decimation matrix, h is the blur point spread function, z is the high resolution image and $n(x)$ is the noise function. Given an approximation u to the high resolution image z, and the image u_0 which is the upsampled version of the observed low resolution image, the residual error is given as

$$r(x) = u_0(x) - (h * u)(x) \quad \ldots (10)$$

Based on the error function, an objective function can be formulated minimization of which gives the high resolution image. The objective function is given as

$$E(u) = \int ((r(x))^2 + \alpha|\nabla u|)dx \quad \ldots (11)$$

The solution for super-resolution from a single image can be given in terms of the following objective function. Here the first term is the data term and the second term is the L_1 (TV) regularization term. The choice of TV norm has found favor in the image restoration community because it allows discontinuities in its solution. As opposed to the L_2 norm it does not smoothen the image across edges. Our motivation for the use of TV based regularization stems from its edge preserving property which is vital for super-resolution. However, the current formulation of data term and regularization term results in a solution that preserves strong edges, however, the finer details of texture are lost in the solution of the above objective function. This can be easily understood by considering the following argument. If there exists a weak edge (the magnitude of gradient is small), then the regularization constraint gives it a low weight. The data fidelity constraint, due to the averaging nature of the blurring kernel, would also not enforce the preservation of the edge. In the iterative energy minimization approach these finer details are therefore lost. In order to preserve texture details and finer details it is required to consider an additional data fidelity constraint. This constraint we formulate as a correlation constraint over various sub-bands of an image. The objective function we use is then

$$J(u) = \int_{\Omega} |\nabla u| \, dxdy + \frac{1}{2}\alpha \int_{\Omega} (u * h - u_0)^2 \, dxdy + \frac{1}{2}\sum_k \lambda_k \int_{\Omega_k} \left(\tilde{U_k} - U_{0k} \right)^2 dvdw \quad \ldots (12)$$

Where, *u* denotes the HR restored image, h is the blurring kernel, u_0 is the interpolated version of the input LR image, $\tilde{U}_k$ denotes the k[th] spectral subband of the estimated LR image formed under the known decimation model in the Fourier domain, U_{0k} is the K[th] sub-band of the input LR image and λ_κ is the corresponding weighing term for the regularizer. Thus an interpolation of the LR observation serves as the initial estimate of the HR image.

3.5.1 Implementation Details:

The objective function given in equation (12) is minimized by an iterative gradient descent technique as done commonly in the literature [38]. The corresponding Euler Lagrange equation for the objective function is given by

$$\frac{\partial}{\partial x}\left(\frac{u_x}{\sqrt{u_{x^2}+u_{y^2}}}\right)+\frac{\partial}{\partial y}\left(\frac{u_y}{\sqrt{u_{x^2}+u_{y^2}}}\right)-\alpha(u*h-u_0)-D^{-1}\Im^{-1}\sum_k\lambda_k\left(\tilde{U}_k-U_{0K}\right) \quad \ldots (13)$$

$$=0, x,y\in\Omega$$

$$\frac{\partial u}{\partial n}=0 \text{, on the boundary of } \Omega=\partial\Omega \quad \ldots (14)$$

The resultant iterative updation process is given by

$$u^{(n+1)}=u^{(n)}+\Delta t\left(\nabla.\frac{\nabla u}{|\nabla u|}+\alpha(u_0-u*h)+D^{-1}\Im^{-1}\sum_k\lambda_\kappa\left(U_{0k}-\tilde{U}_k\right)\right)^{(n)} \quad \ldots (15)$$

Where D^{-1} is the upsampling process and $\Im^{-1}$ implies the inverse Fourier transform. Under this framework, it then becomes possible to assign different weights (λ_κ) to existing error terms in different bands. As opposed to other schemes that we have discussed before, the additional constraint term is calculated and weighed in the spectral domain. The inverse Fourier transform is then applied and finally it is scaled to match the high resolution image dimensions.

It may be argued here that it follows from Parseval's theorem that calculating error power in the spatial domain and the frequency domain should be equivalent. However, the operation in the spectral domain makes it easy to split an image into separable components based on spectral contribution. The number of spectral bands *k* does affect the quality of super-resolution. In general, the higher the number of spectral bands, more the flexibility for preserving details.

We have experimentally tried the method with k= 2 and 4 spectral bands. Under the absence of noise, we use a higher weight factor (λ_κ) for the higher spectral bands which capture the finer details and the edges of the image. Using such a model it is then possible for us to enforce that more importance is given to data fidelity at the

edges. This should ensure that the image that is formed is a sharper super-resolved image of the input LR observation under the known image decimation model. On the other hand, noise in an image can be expected to be captured in the higher frequency sub-bands, which necessitates the use of smaller weights for higher sub-bands when the input image is noisy. An appropriate choice of λ_k would ensure a proper trade-off between the sharpness of the super-resolved image and the accentuation of the noise present. We have experimented with both noisy and noiseless cases and the results are discussed in following section. An interesting enhancement to the work is when the parameter λ_k is related to the concept of wiener filter. Since the wiener filter is an optimal linear filter, the choice of λ_k based on his filter allows us to clean the presence of noise in the data. The details of the procedure are given as an appendix.

3.5.2 Sample Results

As shown in Fig.10 (b) &(c), we can see that the total variational deblurring performed on the bicubic reconstruction sharpens the image at edges but at the cost of loss of the texture. This is not the case for Fig.10 (d) & (e). This can be noted from the presence of texture in the hat and the hair, even though the overall reconstruction remains sharp. This is specifically what we wanted to achieve by our method.

Fig.10 SR using proposed TV based approach for 2x zoom: (a) Input LR image, (b) bicubic interpolated image used as the initial estimate, (c) TV based deblurring of (b), (d)super-

resolution using modified TV based approach using only 2 bands, (e) reconstruction using 4 bands.

4. Experiments on Super-Resolving Images of Material Surfaces

We have used material surface images provided by AFRL/ML. These were metal alloy microscopic and AFM images of a coin as shown in fig.11 below.

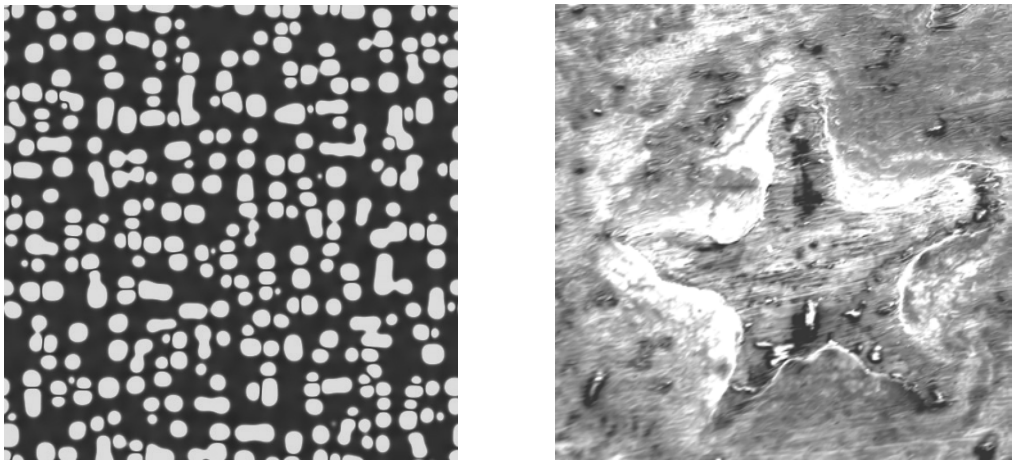

(a) (b)

Fig.11: Material surface image datasets: (a) metal surface image and (b) coin image.

We have named material surface image shown in fig.11(a) as data set 1 and coin image shown in fig.11(b) as data set 2.The super-resolution techniques described in section 3, have been applied on a family of images made available from the AFRL/ML partners. The data set 1 images are of size: 512x512 pixels and the size of data set 2 images are of 800x800 pixels. In addition, a single high resolution scan of a material surface image of size 4kx4k pixels was also used to generate a family of LR images.

4.1. Experiment on data set 1:

Now we show the results of proposed techniques on data set 1. For verification purpose we have downsampled the high resolution (HR) image and downsampling was achieved by skipping pixels. Thus, a downsample by a factor of 2 would involve skipping alternate columns and alternate rows concurrently.

We have used HR images of size 512x512 and formed low resolution (LR) image of size 256x256 as shown in fig.12 (b) below. This LR was processed using various super-resolution techniques.

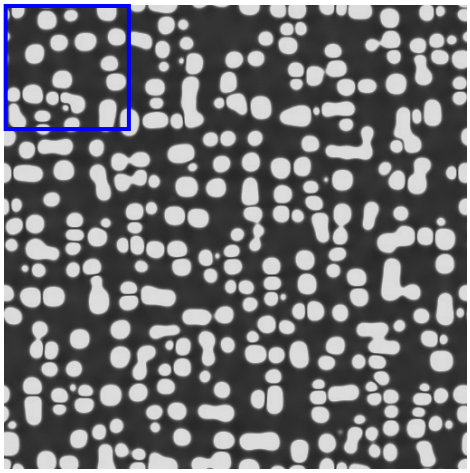

(a) HR

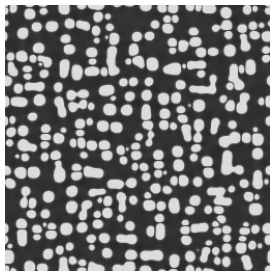

(b) LR

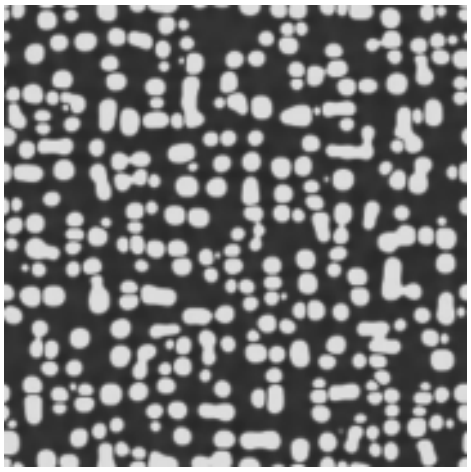

(c) Bicubic

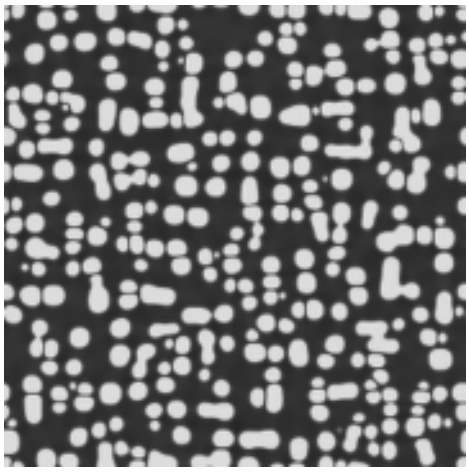

(d) PG

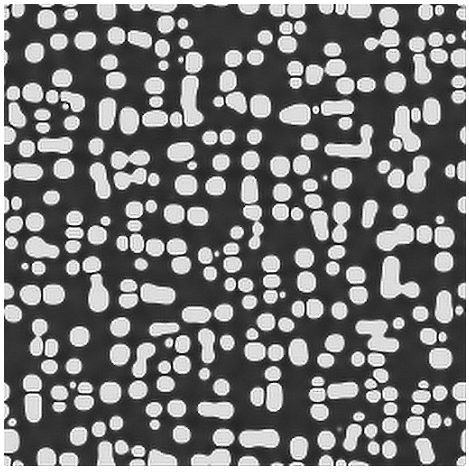

(e) Edge Model

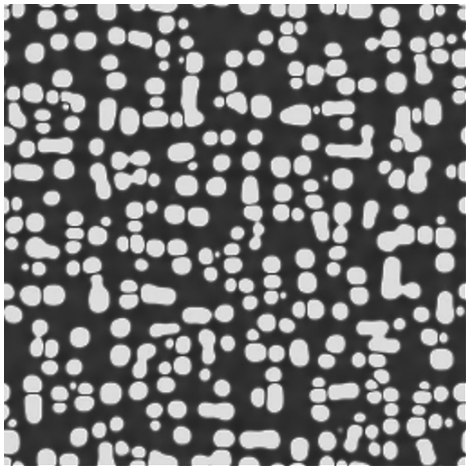

(f) TV

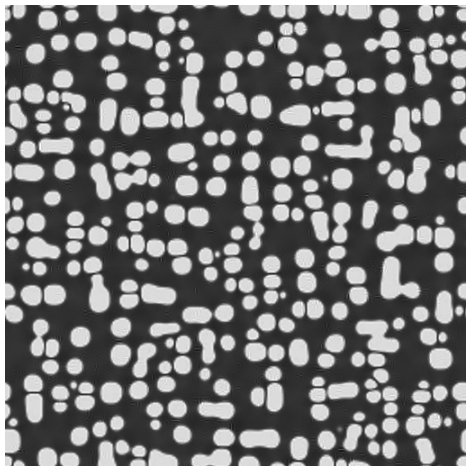

(g) Contourlet

Fig.12. Super-resolution of material surface data set 1: (a) Original HR image of size 512x512 used for comparison, (b) LR image of size 256x256 formed by downsampling the image (a) by factor 2 and used as input, (c) bicubic interpolated image, (d) super-resolved by PG method, (e) super-solved image using edge based model, (f) super-resolved image using total variation approach, (g) super-resolved by contourlet method.

For enhanced visual interpretation of super-resolved images, we cropped a specific region as shown in fig.12 (a) for each super-resolved image. These images are shown below.

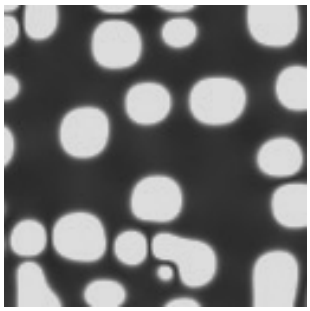

(a) HR

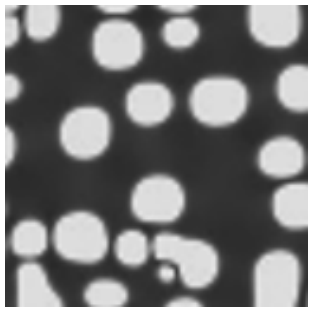

(b) Bicubic

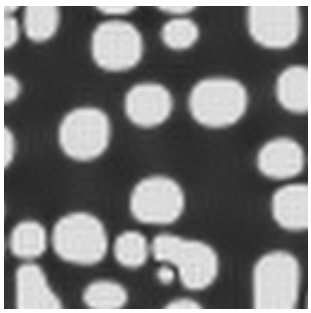

(c) PG

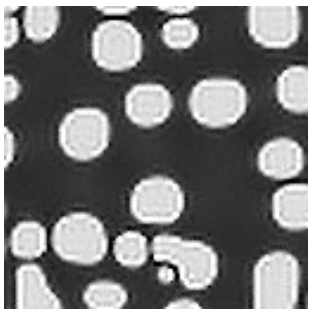

(d) Edge

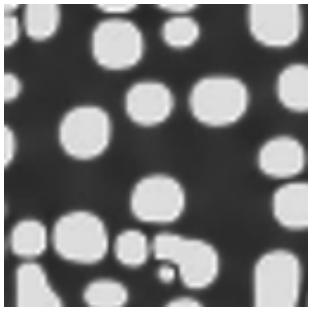

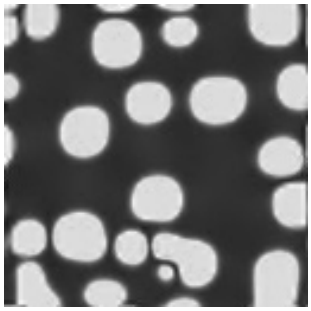

(e) TV (f) Contourlet

Fig.13 (a) original HR image (b) bicubic interpolated image which is quite blurred, (c) Image super-resolved by PG method looks quite smooth,(d) Image super-resolved by edge model appear sharper at edges ,(e) total variation based SR image, (f) Image processed by contourlet approach appears to be superior.

Fig.13 (b) indicates that bicubic interpolation does not yield good result as it produces in blurring the edges. LR image was also processed by PG algorithm which yields fairly better result. It filtered out the high frequency noise and offers a smooth image when processed for 50 iterations. Fig.13 (d) clearly depicts the strong edges present in the super-resolved Image. An analysis indicates that this edge based method does the best for isolated edges. In regions having dense edges, the model seems to perform poorly and leading to ghosting in the generated image.

For total variation method, we take a single LR image and the initial starting image as the bicubic interpolation of the input LR image. The image at every iteration of the restoration process is decomposed into two bands and based on the theory presented above we apply a higher weight to higher frequency component of the image. For the results shown here using a decomposition into only 2 bands, we use the values $\lambda_1 = 0.6$ and $\lambda_2 = 0.8$ and run for 10 iterations. A higher index of λ value implies a higher frequency band. In Fig.13 (e) we can see that the total variational deblurring performed on the bicubic reconstruction sharpens the image. It can be noted that the overall reconstruction remains sharp. This is specifically what we wanted to achieve by our method.

Fig.13 (f) shows the results of the contourlet approach carried out on an LR image shown in Fig.13 (b). For this method we have used 64 images as sample database, all these images were material surface images. The super-resolved image using the proposed approach seems to be much sharper compared to the results of bicubic interpolation. In particular, the edges are better preserved in the super-resolved image using contourlet learning than the bicubic interpolated image where it appears to be more blurred. The super-resolved image compared very favorably to the original high-resolution image.

4.2. Experiment on data set 2:

We applied all proposed techniques on data set 2. Fig.14 (a) shows the original high resolution image used to judge the efficacy of various proposed techniques. We have used HR images of size 800x800 and formed low resolution (LR) image of size 400x400.Fig.14 (b) is the downsampled LR image of fig.14 (a). This LR image was processed by various super-resolution methods.

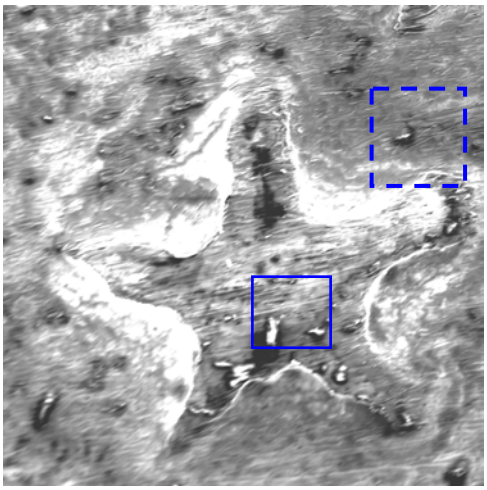

(a) HR

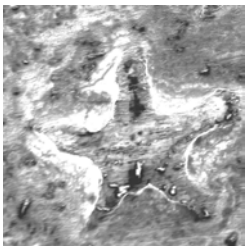

(b) LR

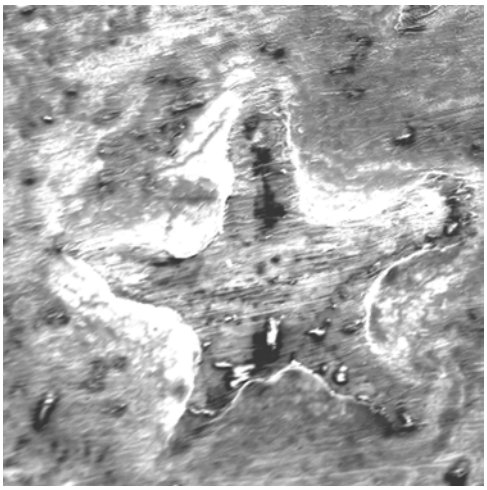

(c) Bicubic

(d) PG

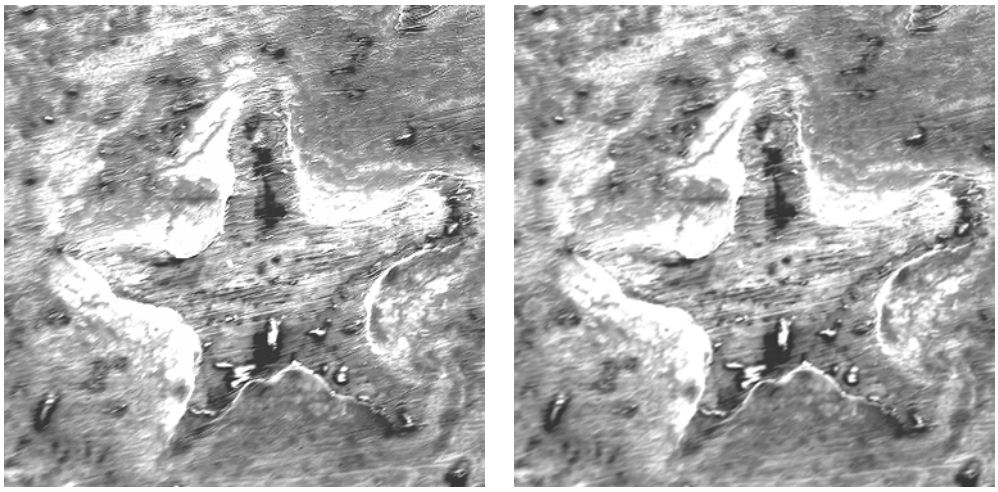

(e) Edge Model (f) TV

(g) Contourlet

Fig.14. Super-resolution of data set 2:(a) original HR image of size 800x800 used for comparison, (b) LR image of size 400x400 formed by downsampling the image (a), (c) bicubic interpolated image of (b), (d) super-resolved image of (b) by PG method, (e) super-solved image of (b) using edge based model, (f) super-resolved image of (b) using total variation approach, (g) super-resolved by contourlet learning method.

To analyze at the smallest details of image, we have cropped all the images for different regions as marked on in fig.14 (a).

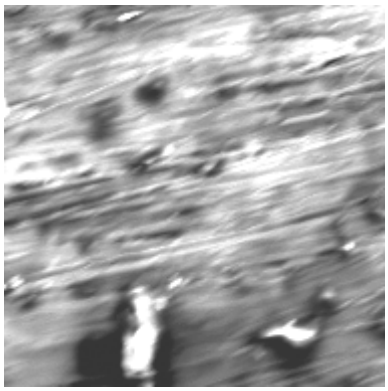

(a) HR

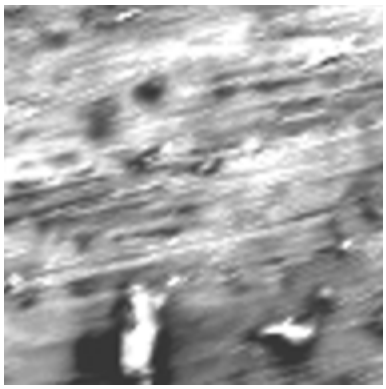

(b) Bicubic

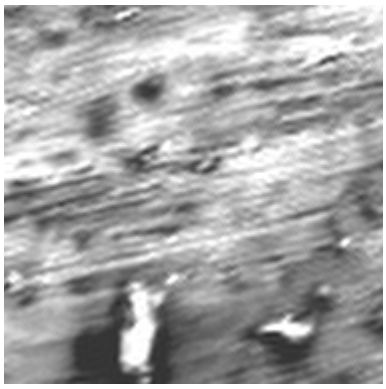

(c) PG

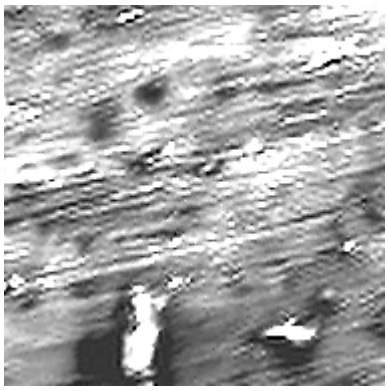

(d) Edge model

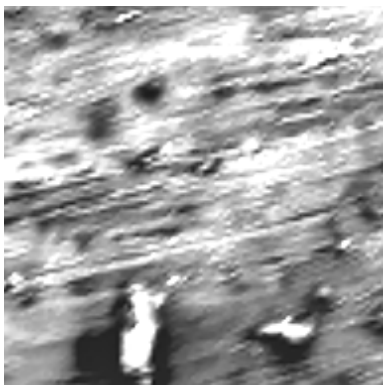

(e) TV

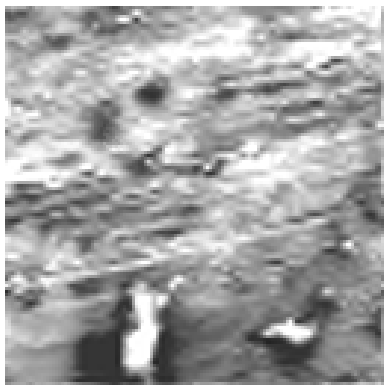

(f) Contourlet

Fig.15: Cropped center part of the image in fig.14: (a) original HR image, (b) bicubic interpolated image which is quite blurred, (c) Image super-resolved by PG method shows lines very clearly compared to previous image, (d) Results by edge based model yields many spurious edges, (e) Image super-resolved by TV method consists of more texture details than other methods, (f) Super-resolution by contourlet approach is better than (e) but inferior to (e).

Fig.15 (b) indicates that bicubic interpolation does not yield a good result as it produces a blurred image. LR image was also processed by Papoulis-Gerchberg algorithm as shown in fig.15 (c) The PG method produces fairly good details about coin surface, still it is not satisfactory.

For Total variation based experiment we take a single LR image and the initial starting image as the bicubic interpolation of the input LR image for total variation. The image at every iteration of the restoration process is decomposed into two bands and processed as discussed in previous subsection. As shown in fig.15 (e) it can be noted that the overall reconstruction remains sharp. As there are no sharp edges present in the original image, the edge model does not deliver a good result as shown in fig.15 (d).

Fig.15 (f) shows the processed image by contourlet approach, where 64 such arbitrary HR coin images are used as the HR training data set. However, the corresponding reconstruction is far from being satisfactory.

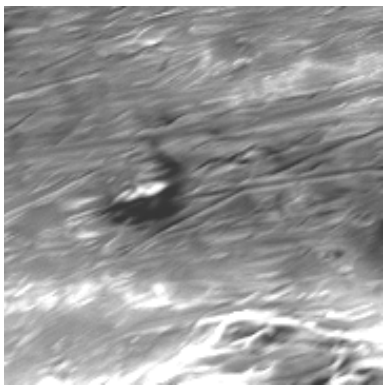

(a) HR

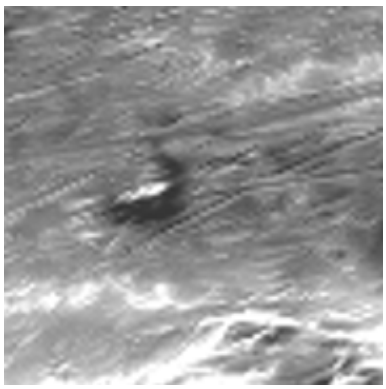

(b) Bicubic

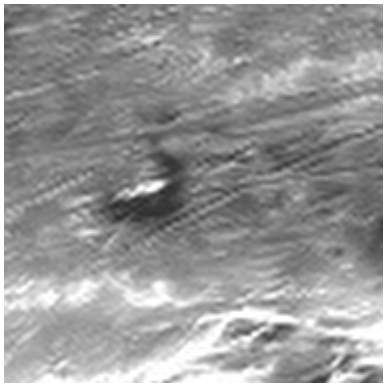

(c) PG

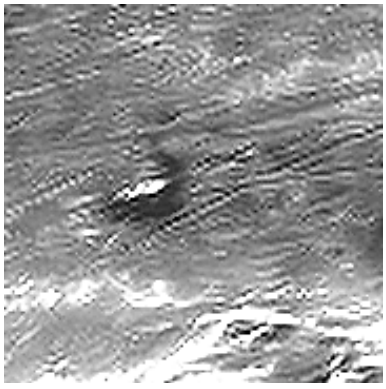

(d) Edge model

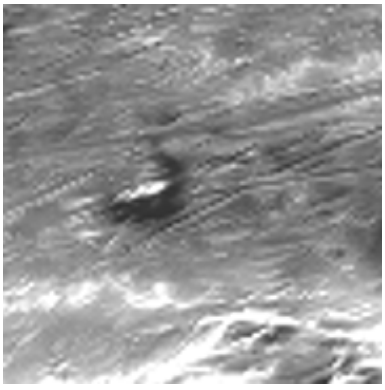

(e) TV

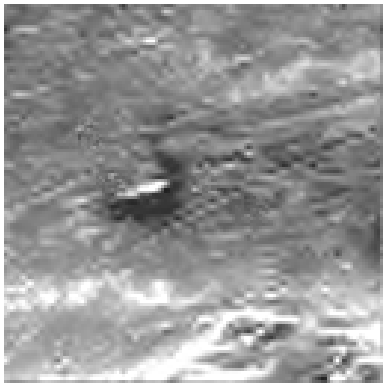

(f) Contourlet

Fig.16: Cropped upper right part of the image in fig.14: (a) original HR image, (b) bicubic interpolated image which is quite blurred, (c) Image super-resolved by PG method looks quite smoother than others, (d) Results by edge based model yields many spurious edges, (e) Image super-resolved by TV method consists of more texture details than other methods, (f) Super-resolution by contourlet approach is better than (e) but inferior to (e).

5. Error Analysis:

Image reconstruction error measurement techniques are used to quantify the quality of reconstruction. Since in this case the original high-resolution image is known, the peak signal to noise ratio (PSNR) can be calculated between original HR image and proposed super-resolved image.

PSNR is defined via mean squared error (MSE) between the original and super-resolved image of size m x n.

$$MSE = \frac{1}{mn}\sum_{i=0}^{m-1}\sum_{j=0}^{n-1}\left\| Z(i,j) - \hat{Z}(i,j)\right\|^2 \quad \ldots (16)$$

where $\hat{Z}$ is super-resolved image, Z is the original image. Now PSNR is defined as,

$$PSNR = 10log_{10}\left(\frac{255^2}{MSE}\right)dB \quad \ldots (17)$$

where 255 is the maximum possible value of a pixel for 8-bit representation. We have calculated the PSNR for all proposed techniques and it summarized in the table below:

Sr. No.	Method Used	PSNR for data set 1	PSNR for data set 2
1	Bicubic Upsampling	24.51	27.17
2	PG Method	31.99	30.07
3	Edge Model Based Method	22.76	21.99
4	Total Variation Approach	22.88	25.66
5	Contourlet Approach	30.76	26.66

Table 1 shows PSNR for Dataset 1and 2 for various super-resolution techniques.

As shown in the Table1above, PSNR of PG method for the metallic surface dataset 1 is 31.99dB, and that of the bicubic interpolation method inferior by 7.48dB. Contourlet learning produces a very good PSNR of 30.76dB for the data set1. For data set 2 also, the PG method yields a better PSNR compared with other methods. The above PSNR values correspond to the input images shown in Figures 12 and 14 only.

Dataset1 images	Bicubic	PG	Edge	TV	Contourlet
1	24.510	31.990	22.760	22.880	31.093
2	24.740	32.010	23.022	23.123	30.932
3	24.600	31.767	22.798	23.001	30.728
4	24.580	31.846	22.698	22.911	30.729
5	24.792	31.867	22.773	23.149	30.740
6	24.722	31.972	23.000	23.085	30.747
7	24.659	31.880	22.965	23.059	30.736
8	24.666	31.799	22.862	23.033	30.828
9	24.605	31.942	22.939	22.998	30.844
10	24.574	31.865	22.842	22.987	30.754
11	24.580	31.809	22.864	22.970	30.617
12	24.688	31.863	22.946	23.068	30.705
13	24.564	31.844	22.769	22.956	30.655
14	24.525	31.676	22.792	22.913	30.670
15	24.657	31.827	22.872	23.036	30.750

Table 2 shows PSNR values for dataset1 super-resolved images (in dB).

Dataset2 Images	Bicubic	PG	Edge	TV	Contourlet
1	23.225	25.168	17.953	22.115	24.742
2	21.544	22.980	16.324	20.548	22.912
3	28.103	32.400	24.767	26.757	29.487
4	34.059	37.542	31.808	32.328	31.821
5	23.820	26.923	18.900	22.640	25.530
6	33.137	36.755	29.914	31.774	31.493
7	29.552	36.028	27.382	27.916	30.810
8	31.947	34.512	29.399	30.180	30.968
9	17.940	18.702	12.657	17.227	18.378
10	26.923	29.954	22.215	25.465	28.801
11	27.776	32.303	24.144	26.255	29.840
12	20.282	20.935	14.836	19.409	21.060
13	24.123	25.955	18.886	22.957	25.615
14	26.772	30.715	22.057	25.171	28.908
15	26.818	30.148	21.788	25.334	28.969

Table 3 shows PSNR values for dataset2 super-resolved image (in dB).

Since we had access to more data (sample images of material surfaces given to us), we analyzed a number of them and produce the corresponding PSNR figures achieved for all these methods in Tables 3 and 4. From Table 2 we notice that the PSNR values for images belonging to category 1 (see Fig 11(a)), are very consistent in all cases. However, the same cannot be said about the results obtained for the images belonging to category 2 (see Fig 11(b)), suggesting certain non-robustness of the proposed method. Notwithstanding above, we do see from Table 3 that the PG method provide a reasonable level of accuracy in most cases. However, it must be mentioned that PSNR is not necessarily a good measure of quantifying the visual quality of reconstruction in case of image Super-Resolution [39] as the measure is heavily biased towards the measuring the contributions from low frequency components.

The performance analysis of the super-resolution techniques is usually estimated by calculating absolute difference between original and super-resolved image. A well designed algorithm should result in a disparity which is essentially made of white noise. At the very minimum, there should be no pattern in the disparity map which correlates with the output or the input. To visually inspect if these characteristics are satisfied, we have chosen to use a hybrid technique comprised of gray-scale modification and pseudo coloring. Instead of showing the errors in normal range, we emphasized the range by using formula,

$$error = max\left(orig - SR\right) \times \sqrt{\left(\frac{\left(orig - SR\right)}{max\left(orig - SR\right)}\right)} \qquad \ldots (18)$$

Where *orig* is the original HR image, *SR* is the super-resolved image. The gray-scale rescaling will give more emphasis for pixels where the error is low, and de-emphasize pixels where the disparity is higher. In essence, this is a histogram equalization strategy for images whose grayscale distribution is laplacian, as is the case with most disparity images.

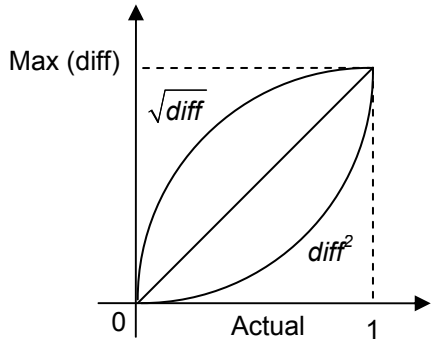

Fig.17: Illustration of how the lower range of error is emphasized for enhanced visualization of the absolute error between the original high resolution image and the super-resolved results.

In figure 18, we see that the highest errors occur in short stretches of curves which resemble the boundaries in the original image. Similar observations can be made about 18c and 18d. The PG method, however, produces acceptable low errors, albeit with a pattern that resembles with boundaries of the high resolution image. It indicates that higher frequency spectral components could still be improved, by increasing the iteration count, albeit at the risk of affecting the location and sporadicity of large disparities across the image. Especially if the point-spread function (PSF) of the diffraction limited imaging source is known precisely, it will result in better choices of parameters involved in running the PG method. On the other hand, figure 19e indicates that contourlet approach is equally suitable for this type of data, when applied on the cropped images. Figures 21, 22 and 23 depict the disparity data for the coin-data images. The PG method produces disparity that is less number of pixels with highest error values, and that too without a pattern.

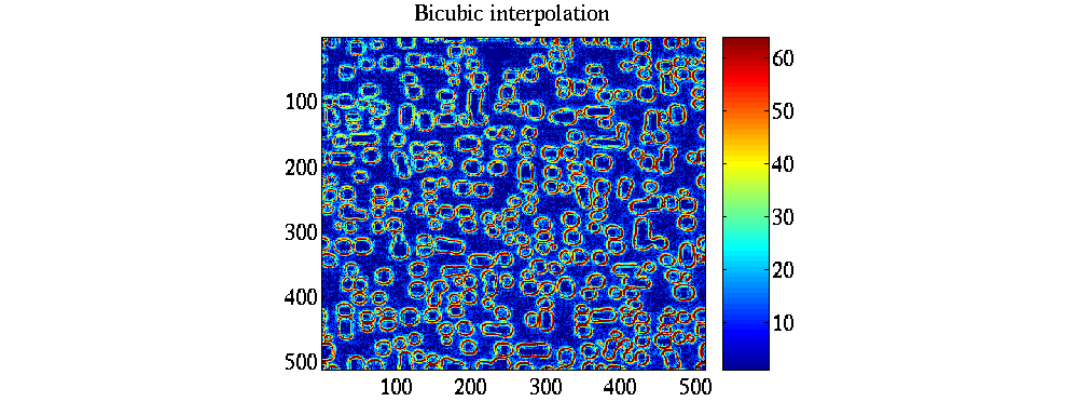

(a)

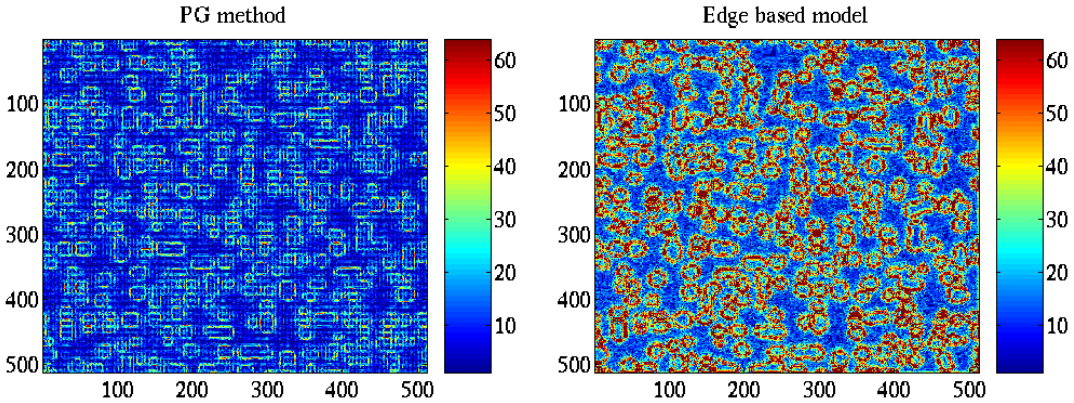

(b) (c)

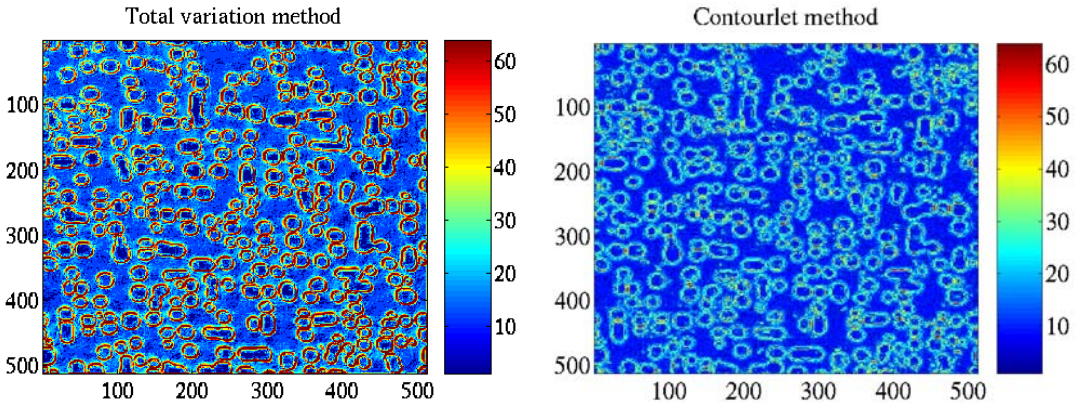

(d) (e)

Fig. 19 Error images of super-resolution techniques shown in fig.12: (a) bicubic interpolated error image, (b) super-resolved by PG method, (c) Edge based model, (d) Total variation approach,(e) contourlet approach.

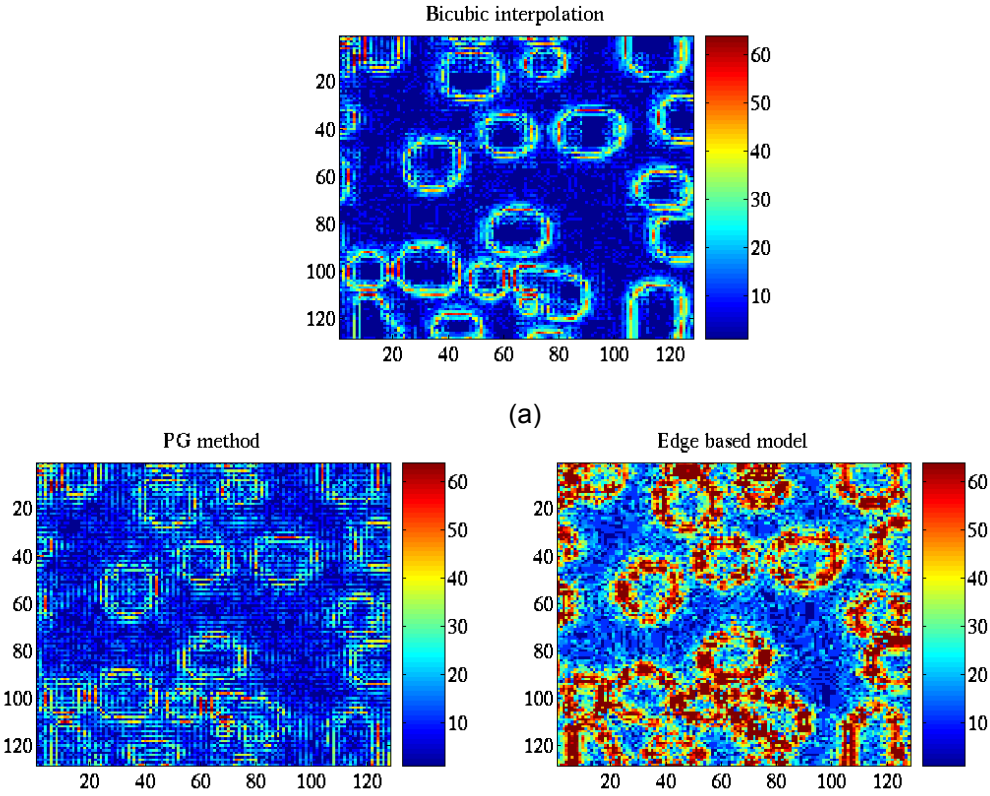

(a)

(b) (c)

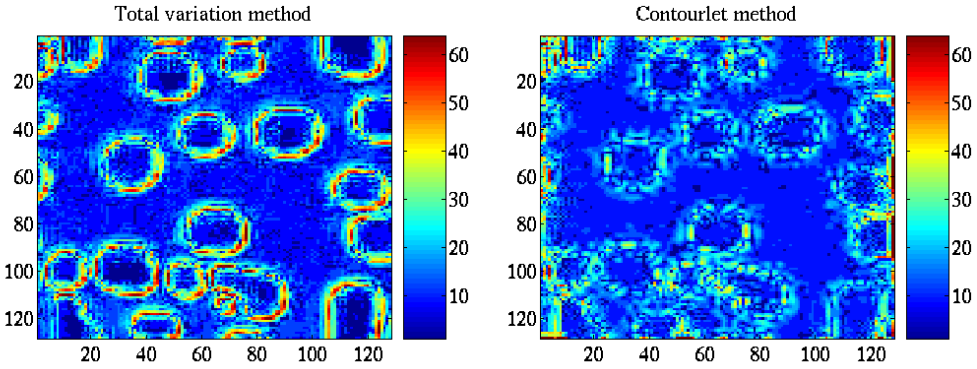

(d) (e)

Fig. 20 Error images of super-resolution techniques shown in fig.13: (a) bicubic interpolated image,(b) PG method, (c)edge based model, (d) total variation method, (e)contourlet approach.

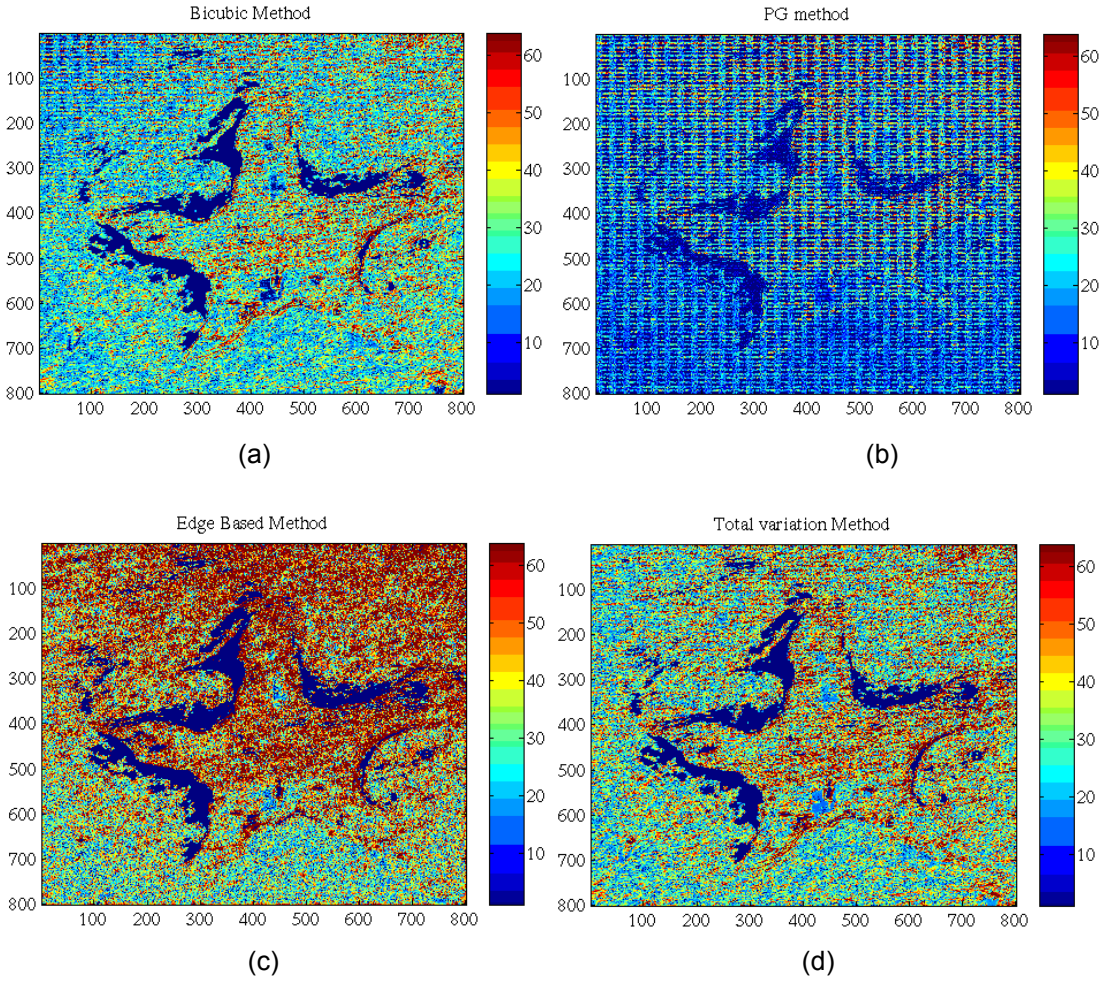

(a) (b)

(c) (d)

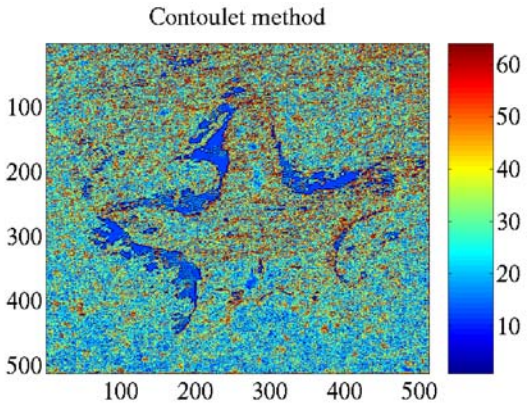

(e)

Fig. 21 Error images of super-resolution techniques shown in fig.14: (a) bicubic interpolated error image, (b) super-resolved by PG method, (c) Edge based model, (d) Total variation app. (e) Contourlet approach.

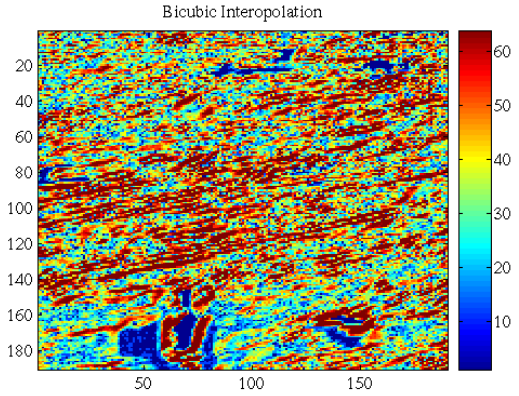

(a)

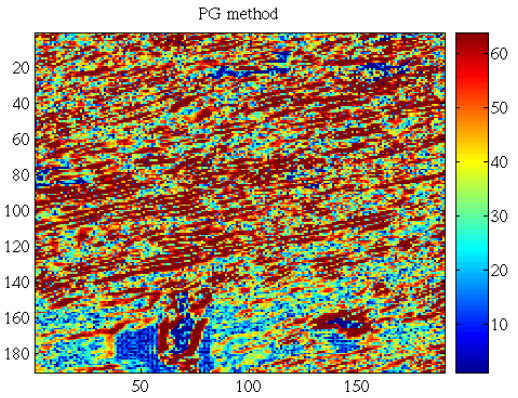

(b)

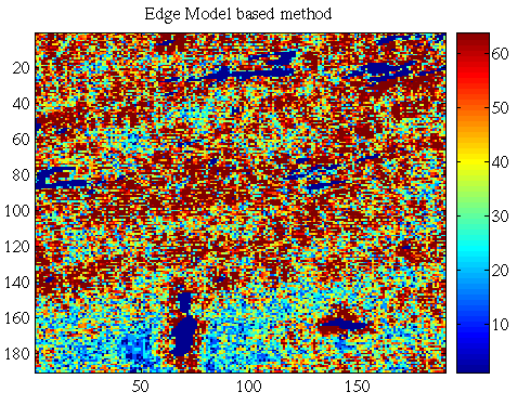

(c)

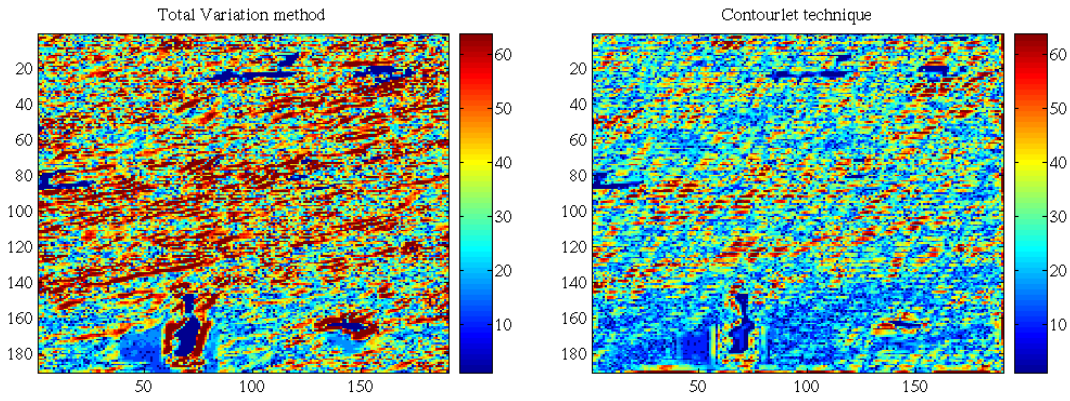

(d) (e)

Fig.22 Error images of super-resolution techniques shown in fig.15 :(a) bicubic interpolated image, (b) PG method, (c)edge based model, (d) total variation method, (e)contourlet approach.

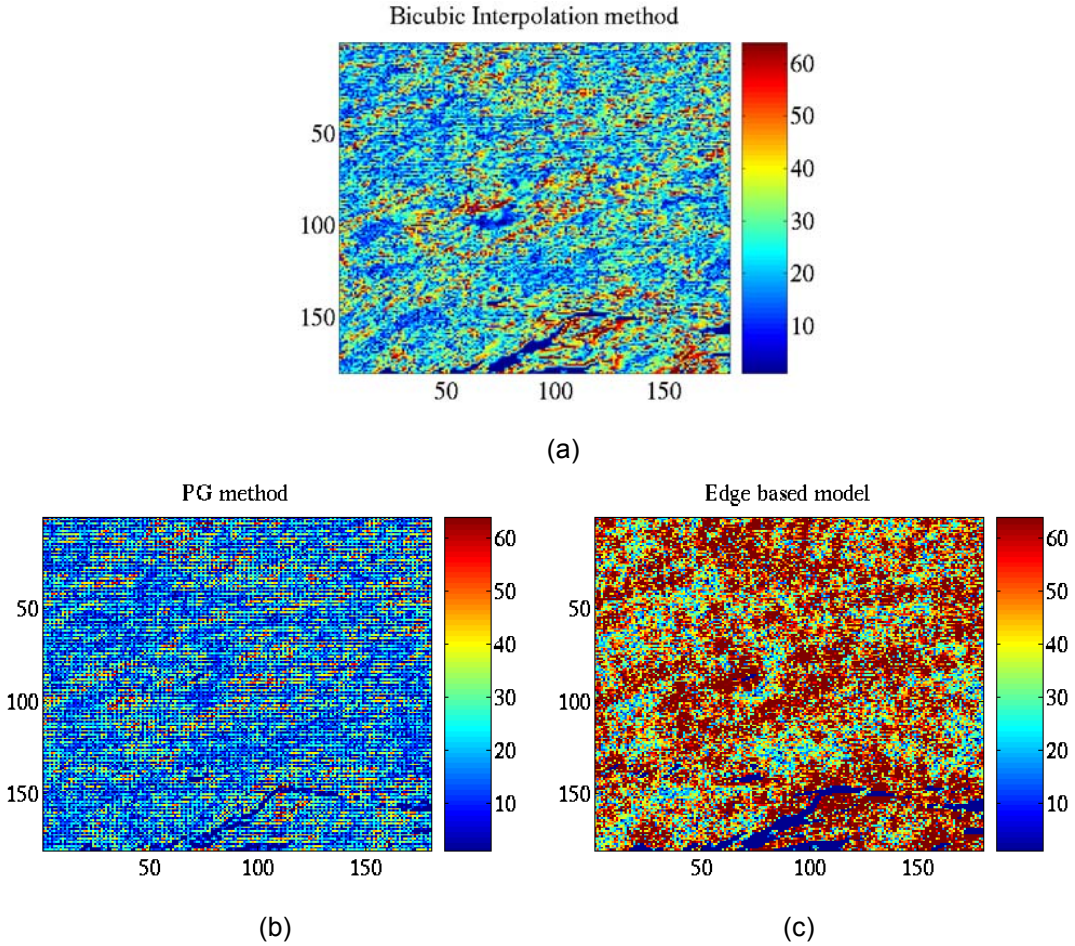

(a)

(b) (c)

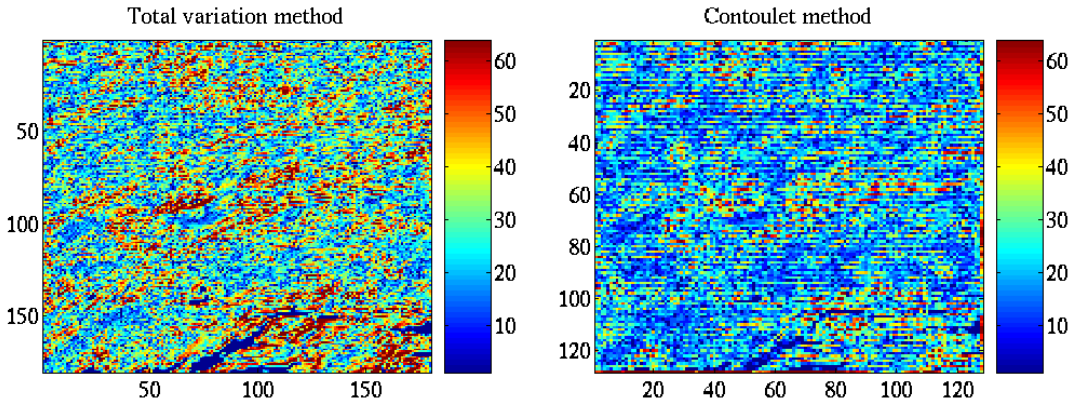

(d) (e)

Fig.23 Error images of super-resolution techniques shown in fig.16 :(a) bicubic interpolated image, (b) PG method, (c)edge based model, (d) total variation method, (e)contourlet approach.

6. Conclusions:

We have explored various methods for super resolution of material surface images as well as other images in the report. Based on observations we recommend the usage of either the contourlet based method or TV based approach for super-resolving optical microscope data. To super-resolve the AFM data, we recommend the usage of either TV-based approach or PG method.

7. References:

1) R.Y. Tsai and T.S. Huang, "Multiframe Image Restoration and Registration", in
Advances in Vision and Image Processing, pp. 317-339. JAI Press Inc., 1984.
2) M. Irani and S. Pelag, "Improving resolution by image registration," *CVGIP: Graphical Models and Image Processing,* vol. 53, pp. 231-239, March 1991.
3) M. Irani and S. Pelag, "Motion Analysis for Image Enhancement: Resolution, Occlusion, and Transparency,' *VCIR*, vol. 4, pp. 324-335, December 1993.
4) A.M. Tekalp, M.K. Ozkan and M.I. Sezan, "High Resolution Image Reconstruction from Lower-Resolution Image sequences and space- Varying Image restoration," in *Proc.IEEE Int.conf. on Acoustics, Speech, and Signal Processing,* San Franisco, USA, 1992, pp. 169-172.
5) M. K. Ng, N.K. Bose, and J. Koo, "Constrained Total Least Squares Computation for High Resolution Image Reconstruction with Multisensors," *International Journal of Imaging Systems and Technology,* vol. 12, pp. 35-42, 2000.

6) M. K. Ng, N.K. Bose, “Analysis of Displacement Errors in High Resolution Image Reconstruction with Multisensors,” *IEEE Trans. Circuits and Systems I: Fundamental Theory and Applications,* vol. 49, no. 6, pp. 806-813, June 2002.
7) M. K. Ng, N.K. Bose, “Fast colour Image Restoration with Multisensors,” *International Journal of Imaging Systems and Technology,* vol. 12, no. 5, pp. 189-197, 2002.
8) N. Nguyen, P. Milanfar, and G. Golub, “A Computationally Efficient Super-resolution Reconstruction Algorithm,” *IEEE Trans. Image Processing,* vol. 10, no. 4, pp. 573-583, April 2001.
9) R.R. Schultz and R.L. Stevenson, “A Bayesian Approach to Image Expansion for Improved Definition,” *IEEE Trans. on Image Processing*, vol. 3, no. 3, p. 233-242, May 1994.
10) D. Rajan and S. Chaudhuri, “Generation of Super-resolution Images from Blurred Observations using an MRF Model,” *J. Mathematical Imaging and Vision,* vol. 16, pp. 5-15, 2002.
11) D.Rajan and S. Chaudhuri, “Simultaneous Estimation of Super- Resolved Scene and Depth Map from Low Resolution Observations,” *IEEE Trans. on Pattern Analysis and Machine Intelligence*, vol. 25, no. 9, pp. 1102-1117, September 2003.
12) M. Elad and A. Feuer, “Restoration of Single Super resolution Image from Several Blurred, Noisy and Under sampled Measured Images,” *IEEE Trans. on Image Processing*, vol.6, no.12, pp. 1646-1658, December 1997.
13) Z. Lin and H.Y. Shum, “Fundamental Limits of Reconstruction-Based Super-Resolution Algorithms under Local Translation,” *IEEE Trans. on Pattern Analysis and Machine Intelligence,* vol. 26, no.1, pp. 83-97, January 2004.
14) S. Baker and T. Kanade, “Limits on super-Resolution and How to Break them,” *IEEE Trans. on Pattern Analysis and Machine Intelligence,* vol. 24, no.9, pp. 1167-1183, September 2002.
15) D. Capel and A. Zisserman, “Super-Resolution from Multiple Views using Learnt Image Models,” in *Proc. IEEE Int. Conf. On Computer Vision and Pattern Recognition*, 2001, pp. II:627-634.
16) W.T. Freeman, T.R. Jones, and E.C. Pasztor, “Example-Based Super-Resolution,” *IEEE Computer Graphics and Applications*, vo.22, no.2, pp 56-65, March/April 2002.
17) A. Hertzmann, C.E. Jacobs, N. Oliver, B. Curless, and D.H. Salesin, “Image Analogies” in *Proc. SIGGRAPH*, 2001, pp. 327-340.
18) M.V. Joshi and S. Chaudhuri, “A Learning-Based Method for Image Super-Resolution from Zoomed Observations,” in *Proc. Fifth Int. Conf. On Advance in Pattern Recognition* Indian statistical Institute, Kolkata, India, 2003, pp. 179-182.
19) C.V. Jiji, M.V. Joshi and S. Chaudhuri, “Single Frame Image Super-resolution Using Learned Wavelet Coefficients,” *International Journal of Imaging Systems and Technology*, vol. 14, no. 3, pp.105-112, September 2004.
20) B.K. Gunturk, A.U. Batur, Y. Altunbasak, M.H. Hayes, and R.M. Mersereau, “ Eigenface-Domain Super- Resolution for face recognition,” *IEEE Trans. on Image Processing*, vol.12, no. 5, pp. 597-606, May 2003.
21) X. Wang and X.Tang, “Hallucinating Face by Eigen transformation with Distortion Reduction,” in *Proc. Of Int. Conf. on Biometrics Authentication*, Hong Kong, 2004.
22) C.V. Jiji and S. Chaudhuri, “PCA based Generalized Interpolation for Image Super-Resolution,” in *Proc. Indian Conf. on Computer Vision Graphics and Image Processing*, Kolkata, 2004.
23) Lyndsey C. Pickup, Stephen J. Roberts, and Andrew Zisserman, “A Sampled Texture Prior for Image Super-Resolution,” in *Advances in Neural Information*

Processing Systems 16, Sebastian Thrun, Lawrence Saul, and Bernhard Schölkopf, Eds., pp 1587-1594. MIT Press, Cambridge MA, 2004.
24) H. Chang, D.Y. Yeung, and Y. Xiong, " Super-Resolution Through Neighbor Embedding," in *Proc. IEEE Conf. on Computer Vision and Pattern Recognition*, Washington, 2004, pp. 275-282.
25) I.Begin and .P. Ferrie, "Blind Super-Resolution Using a Learning Based Approach," in *Proc. Int. Conf. Pattern recognition, Cambridge,* U.K., 2004, pp. 85-89.
26) J.S. Park and S.W. Lee "Enhancing Low-Resolution Facial Images Using Error Back-Projection for human Identification at a Distance," in *Proc. Int. Conf. Pattern recognition, Cambridge,* U.K., 2004, pp. 346-349.
27) J. Sun, N.N. Zheng, H. Tao, and H.Y. Shum, "Image Hallucination with Primal Sketch Priors," *IEEE Conf. on Computer Vision and Pattern Recognition*, Wisconsin, 2003, pp. 729-736.
28) J. Wu, M. Trivedi, and B. Rao, "Resolution Enhancement by Adaboost," *Proc. Int. Conf. Pattern recognition, Cambridge,* U.K., 2004, pp. 893-896.
29) P. Chatterjee, V.P. Namboodiri and S. Chaudhuri, ``Super-resolution Using Sub-band Constrained Total Variation", *Proc. Intl. Conf. on Scale Space & Variational Methods* (SSVM'07), Ischia, Italy, May 2007.
30) P.Chatterjee, S. Mukherjee, S. Chaudhuri and Guna Seetharaman," Application of Papoulis-Gerchberg Method in Image Super-resolution and Inpainting" to appear in C*omputer Journal, Oxford University Press*.
31) Malay Kumar Nema, S.Rakshit and S.Chaudhuri,"Edge Model Based High Resolution Image Genration*"Indian Conference on Computer Vision,graphics and Image Processing*, Madurai 2006 pp. 1-12.
32) S. Farsiu, D. Robinson, M. Elad, and P. Milanfar, "Advances and Challenges in Super-Resolution", Invited Paper, *International Journal of Imaging Systems and Technology*, Special Issue on High Resolution Image Reconstruction, vol. 14, no. 2, pp. 47-57, August 2004.
33) Athanasios Papoulis, "A new algorithm in spectral analysis and band-limited extrapolation," *IEEE Transactions on Circuits and Systems*, vol. CAS-22, no. 9, pp. 735- 742, September 1975.
34) R.W. Gerchberg, "Super-resolution through error energy reduction," *Optical Acta,* vol. 21, no. 9, pp. 709 -720, 1974.
35) Anil K. Jain, Fundamentals of Digital Image Processing, Prentice Hall of India Private Limited, New Delhi - 110 001, 2001.
36) David O. Walsh and Pamela A. Nielsen-Delaney, \Direct method for super resolution," Journal of Optical Society of America, vol. 11, no. 2, pp. 572- 579, February 1994
37) M. Nema, S. Rakshit and S. Chaudhuri, ``Edge Model Based High Resolution Image Generation", *Proc. Indian Conf. on Vision, Graphics & Image Processing* (ICVGIP), Madurai, Dec. 2006.
38) Rudin, L.I., Osher, S., Fatemi, E.: Nonlinear Total Variation Based Noise Removal Algorithms. Physica D 60 (1992) 259-268
39) S. Chaudhuri and M.V. Joshi, ``Motion-Free Super-Resolution", Springer, NY, 2005.